Effect of Periodic Wake Passing on Film Effectiveness of Inclined Discrete Cooling Holes around the Leading Edge of a Blunt Body

K. Funazaki[1], E. Koyabu[2], S. Yamawaki[3] and T. Maya[3]

ABSTRACT

Detailed studies are conducted on film effectiveness of inclined discrete cooling holes around the leading edge of a blunt body that is subjected to periodically incoming wakes as well as free-stream turbulence with various levels of intensity. The cooling holes have a configuration similar to that of typical turbine blades and are angled at 30 and 90 degree to the surface in the spanwise and streamwise directions, respectively. A spoke-wheel type wake generator is used in this study to simulate periodically incoming wakes to turbine blades. In addition, two types of turbulence grids are used to elevate a free-stream turbulence intensity. We adopt three blowing ratios of the secondary air to the mainstream. Most of the dominant flow conditions are reproduced in this study except for the air density ratio of the secondary air and the main stream. For each of the blowing ratios, wall temperature around the surface of the test model are measured by thermocouples situated inside the model. The temperature is visualized using liquid crystals in order to obtain qualitative information of film effectiveness distribution.

NOMENCLATURE

B	:Mean blowing ratio $=\rho_2 U_2 / \rho_\infty U_\infty$
D	:Leading edge diameter
d	:Cooling hole diameter
d_g	:Diameter of the turbulence grid wire
f	:Wake passing frequency $(=nn_c / 60)$
L	:Axial gap between the turbulence grid and the model leading edge
l	:Axial gap between the wake generator and the model leading edge
L_e	:Streamwise dissipation length of free-stream turbulence
M	:Grid mesh size of the turbulence grid
M_{15}, M_{40}	:Local momentum ratio
Nu_D	:Nusselt number based on the leading edge diameter
n, n_c	:Rotating speed and the number of wake generating bars
R	:Radius of the leading edge
Re_D	:Reynolds number based on the diameter of the leading edge and the inlet velocity$=U_\infty D / \nu$
S	:Strouhal number$=fD / U_\infty$
T, T_{aw}	:Temperature, adiabatic wall temperature
$Tu(t)$	:Turbulence intensity
Tu_b	:Back ground turbulence intensity
U_{local}	:Local flow velocity around the model surface
U_∞	:Inlet velocity
u'	:Streamwise velocity fluctuation
V_{out}	:Outlet velocity
v	:Velocity on the model surface
x	:Axial distance measured from the leading edge
x_{surf}	:Distance along the surface from the stagnation on the leading edge
η	:Film effectiveness $=(T_{aw}-T_\infty)/(T_2-T_\infty)$
Subscripts	
∞,2	:mainstream, secondary air
15,40	:first row, second row

1 Department of Mechanical Engineering,Iwate University, Japan
2 Graduate School, Iwate University, Japan
3 Aero-Engine & Space Operation, Ishikawajima-Harima Heavy Industries Co.,Japan

Presented at 1995 Yokohama International Gas Turbine Congress held in Yokohama, Japan from October 22nd to October 27th, 1995.
Manuscript received at the Organizing Committee on July 10, 1995.

INTRODUCTION

To improve the performance of gas turbines, the specifications for turbine inlet temperature has been increasing during several decades while cooling air flow must be kept to a minimum. For this reason, it is necessary to improve turbine cooling techniques not only for blades in the first stage but also for blades in the subsequent stages. Furthermore, those blade metal temperatures under an actual flow environment must be predicted more accurately.

Film cooling is an effective method for protecting blades surfaces from high temperature combustion gas. There have been many investigations to study the thermo-fluid characteristics of film cooling. Especially the leading edge film effectiveness of turbine blades, which is our concern in this study, have been attracting much attentions from many researchers[1] [2] [3]. This is because heat load around the leading edge is inherently high and it is difficult to cool the leading edge region properly. Meanwhile, as Funazaki et al.[4] pointed out, free-stream turbulence as well as periodic wake passage affected the boundary-layer around the leading edge of turbine blades to great extent, which implied the possible interaction between the film cooling air and those disturbances.

Recently, Funazaki et al. [5] studied the influence of periodically passing wakes as well as free-stream turbulence on the film effectiveness of discrete cooling holes over the leading edge of a blunt body. Their test model had a realistic geometrical configuration of cooling holes except for the injection angle; normal to the surface. They found that the film effectiveness at lower blowing ratio greatly deteriorated due to the wake passing and the free-stream turbulence. Although their findings are quite useful for understanding how the film effectiveness of the leading edge cooling holes behaves under the realistic flow environment, they are not applicable to turbine cooling design in a straightforward manner because of the injection angle adopted in their study.

This study therefore focuses on the effect of periodic passing wakes on film effectiveness of spanwisely-inclined cooling holes on the leading edge under several free-stream turbulence conditions. The model used in this study has the same geometry as the previous study [5], consisting of a semi-circular leading edge and flat afterbody.

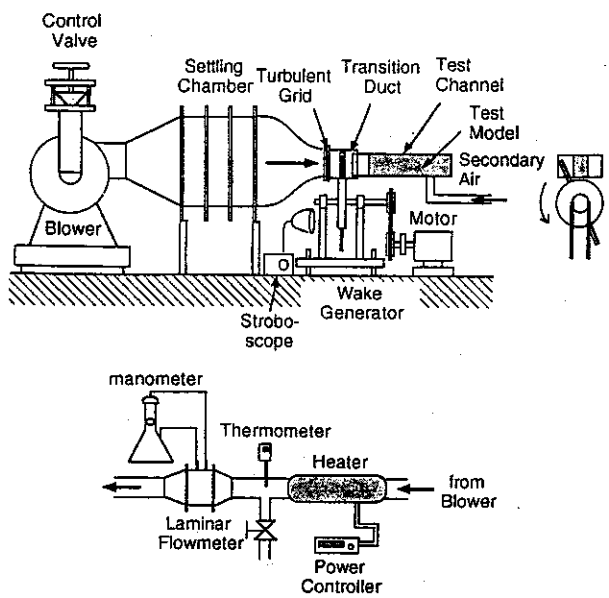

Figure 1 Test apparatus
(upper) Wind tunnel (lower) Secondary air supply system

Table 1 Configurations of turbulence grids and the characteristics of the turbulence generated by each grid

	Grid 1	Grid 3	No Grid
Wire Diameter (dg)	0.8 mm	5.0 mm	-
Mesh Width (M)	5.0 mm	30.0 mm	-
Degree of Openness	0.7	0.69	-
M / dg	6.25	6	-
Tub	1.50%	4.00%	0.80%
Le	2.8 mm	7.8 mm	-

Spanwise angle of each of the cooling holes is 30° measured from the model surface, which is commonly used in modern turbine blades. The upstream periodic wakes is produced by a spoke-wheel type wake generator. The free-stream turbulence is generated by turbulence grids. We adopt three blowing ratios of the secondary air to the mainstream. For each of the blowing ratios, adiabatic wall temperature around the test surface influenced by the wakes as well as the free-stream turbulence is measured by thermocouples.

TEST APPARATUS AND INSTRUMENTS

A schematic layout of the test apparatus is shown in Figure 1. This apparatus is the same as that used in previous study by Funazaki et al. [5]. Main flow rate is adjusted by the inlet valve of the blower. Air from the blower passes through the settling chamber to the contraction nozzle with the exit cross section of 240mm x 350mm. The test channel containing the test model is inserted into the transition duct which is attached the contraction nozzle. To remove the upstream boundary layer, the front portion of the test channel has a sharp-edged and 10 mm clearance with the transition duct. The transition duct has a slot through which the wake generating bars of the wake generator can pass. These wake generating bars, of 5 mm diameter and 250 mm length, are mounted on the disk rim. The rotational speed of the disk is controlled by transmission gear box connected to an induction motor. The rotational speed, ranging from 900 through 1500 rpm, is monitored by a stroboscope. A turbulence grid is attached to the contraction nozzle exit which is 300mm upstream of the test model leading edge and 100 mm upstream of the wake generator. Two types of grids are used and details of the grid configurations are shown in Table 1. It is revealed that these "passive type" grids can generate realistic turbulence

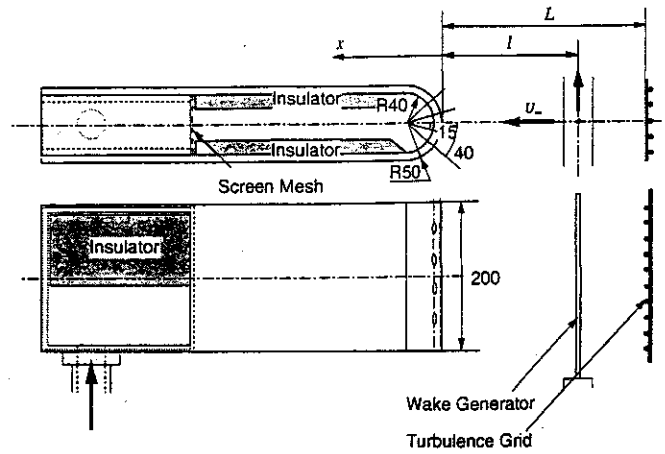

Figure 2 Test model

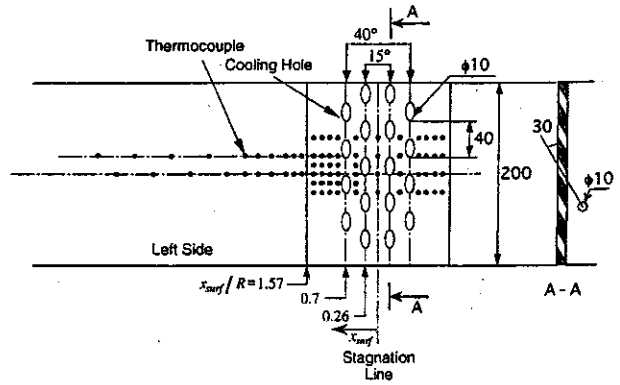

Figure 3 Layout of the film holes and locations of thermocouples on unholded surface view

intensity levels encountered in front of turbine rotor blades [5].

The secondary air supplied from the second blower to the film holes is heated before a laminar-flowmeter. Accordingly, the film air temperature is higher than the free-stream temperature, which means we can not simulate the density ratio of the secondary air to the mainstream air in an actual engine.

The cross section of the test channel is 200 mm height and 300 mm width and its length is 1000 mm. The test model consists of a semi-circular leading edge of 100 mm diameter and a flat afterbody, shown in Figure 2. The test model is assembled with acrylic-resin parts of 10 mm thickness and 200 mm height. Two rows of holes of d=10 mm diameter and 40 mm ($4d$) pitch, located at ±15°and ±40° angled with the test model center line. Axes of the holes are spanwisely inclined by 30°. The ratio of the leading edge diameter and the cooling hole diameter, D/d is 10, We will refer to the film holes at ±15° and ±40° as "the first row" and "the second row", respectively. The test model is lined with some bricks of insulator except for the back surface of the leading edge.

The secondary air is led from the flow settling chamber inside the model to the back surface of the leading edge of the model. Figure 3 shows the location of thermocouples and film holes. The test model has 74 thermocouples embedded on the model surface to measure an adiabatic surface temperature distribution. The secondary air temperature is measured at the middle of the plenum chamber inside the model. A temperature on the back surface of the model are also measured to check the adiabatic wall condition. Free-stream temperature is measured near the lower end of the leading edge stagnation line. All thermocouples are connected to a datalogger controlled by a personal computer. These temperature data are then averaged over 10 samples acquired within a few

minites to calculate time-averaged wall temperature distributions.

Pressure distributions around the test model are obtained using the test model of the same dimensions as the present one except for cooling holes, as had been employed by Funazaki [6]. Local flow velocity U_{local} is then determined from those data.

The temperature distribution is visualized using a liquid crystal sheet of 0.1 mm thickness (RW3040; Nippon Capsule Products). The sheet is pasted around the test model. The color changes in a temperature range of 30~40°C. Due to this broad range, it is difficult to get a sharp image of colored temperature distribution, however, the liquid crystal provides us a brief image about how the injected air spread over the test model, which can be used for interpreting the temperature data from the thermocouples.

EXPERIMENT

In the present study, normalized parameters adopted in this study except for Mach number are comparable to those encountered in a real turbomachine.

The inlet free-stream velocity was about 20m/s and the Reynolds number Re_D was 120000. The rotational speed of the wake generator was 900,1260, and 1500 rpm. The corresponding Strouhal number S, defined as

$$S=\frac{\frac{nn_c}{60}D}{U_\infty}, \tag{1}$$

is 0.24, 0.34 and 0.40.

Unsteady velocity measurements were already conducted using a hot-wire anemometer in the previous study and those data, such as ensemble-averaged velocity or time-resolved turbulence intensity can be directly used in the present study to describe the unsteady flow field around the leading edge of the model.

The blowing ratio B, one of the most dominant parameter for film cooling, is defined as

$$B=\frac{\rho_2 U_2}{\rho_\infty U_\infty}. \tag{2}$$

B is based on the mean secondary air and the inlet flow mass flux. All experiments were conducted at the mean blowing ratios, B=0.4, 0.8, or 1.2. Although this blowing ratio is a convenient parameter for this type of experiment, local blowing ratio at each row is more useful for understanding the local film cooling performance. The local blowing ratio is defined as

$$B_{15}=\frac{\rho_{2,15}U_{2,15}}{\rho_{\infty,15}U_{\infty,15}}, \quad B_{40}=\frac{\rho_{2,40}U_{2,40}}{\rho_{\infty,40}U_{\infty,40}}. \tag{3}$$

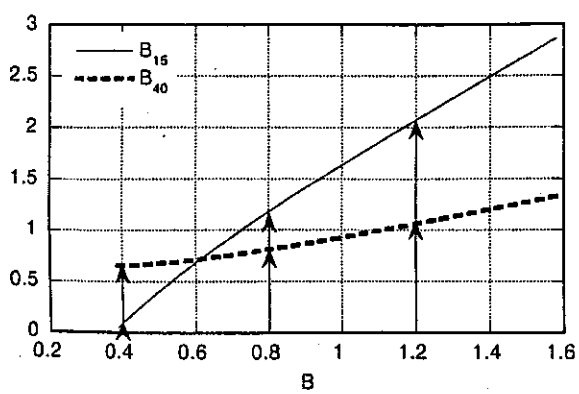

Figure 4 Relationship of local and mean blowing ratio

Figure 4 shows the analytical result of the relationship between the local and mean blowing ratios, indicating that these relationships differ for each row. For instance, for B_{15}, the slope of the curve is about 2.5 and $B_{15} >> 1$ when $B \geq 0.8$. In contrast, for B_{40}, the slope is about 0.5 and $B_{40} \leq 1$ even when $B \leq 1.2$.

Film effectiveness η is defined as

$$\eta=\frac{T_{aw}-T_\infty}{T_2-T_\infty}, \tag{4}$$

where T_{aw} is the adiabatic wall temperature, T_2 is the secondary air temperature, and T_∞ is the mainstream temperature. During the experiment, the temperature difference $T_{aw}-T_w$ was maintained about 20K. Since it is actually difficult to achieve a sufficiently adiabatic wall condition in this test model, some correction must be made on the results of Eq. (4). Although rigorous correction seems almost impossible, the method used by Mick and Mayle[7] are adopted, in which Eq. (4) can be modified as follows;

$$\eta=\frac{T_{aw}-T_\infty}{T_2-T_\infty}=\frac{T_m-T_\infty-\Delta T}{T_2-T_\infty}+\frac{q_{rad}+q_{cond}}{h(T_2-T_\infty)}, \tag{5}$$

where T_m is the measured surface temperature, ΔT is the surface temperature correction, h is the heat transfer coefficient influenced by the injected air, q_{rad} and q_{cond} are the radiative and conduction heat flux from the surface, respectively. ΔT consists of two parts; one is the effect of back surface heating and the other is the effect of ill-positioning of the hot junctions of the thermocouples. The magnitude of the latter effect was determined by the preliminary test. The former effect seems to depend on the temperature difference between the front and back side of the test model (T_2-T_w). In this study, on a basis of the finding by Mick and Mayle[7], it is assumed that the magnitude of ΔT is about 5% of (T_2-T_w). For simplicity, we also assume that q_{rad} and q_{cond} cancel each other.

An uncertainty analysis based on the method of Kline and McClintock [8] was carried out for the film effectiveness. The uncertainty of film effectiveness, including the effects of the above-mentioned assumptions, is about 6% over the leading edge region except for the rim regions of the cooling holes and less than 12% for downstream.

RESULTS AND DISCUSSION

Velocity Distribution

Figure 5 shows the experimental results of the velocity

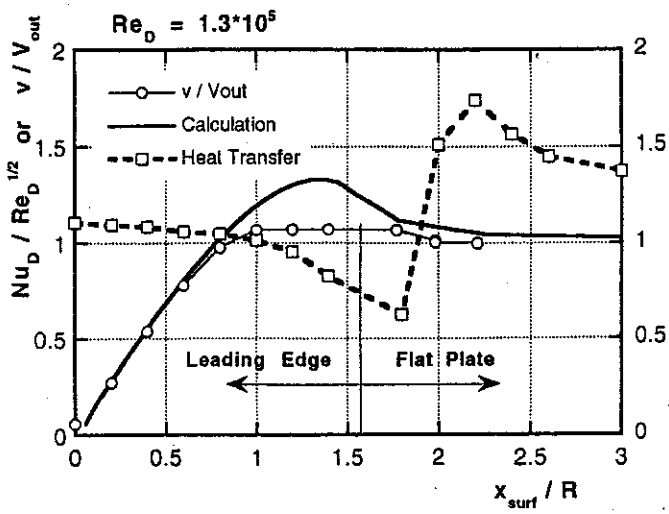

Figure 5 Velocity and heat transfer distributions

distribution as well as the heat transfer distribution ($Nu_D/Re_D^{0.5}$) around the leading edge of the test model, accompanied by the corresponding potential flow analysis by use of BEM (Boundary Element Method). These data show that there was a separation bubble around the junction of leading edge and flat plate. The separation began at $X_{surf}/R \cong 1$ and reattached at $X_{surf}/R \cong 2$.

It should be noted that these data were for the test model with no cooling holes. In fact, cooling holes or injected air have some influence on the boundary layer over the leading edge, which seems to affect the separation to some extent. To the author's best knowledge, no information is available on this point, therefore the data in Figure 5 is used as an indicator of a separation bubble. Besides, detailed measurements on the behavior of separation bubble under several disturbances are scheduled to obtain some insight into this phenomena.

Free-Stream Turbulence and Wake Turbulence

Free-stream turbulence as well as wake turbulence were already measured in the previous study [5] by use of a hot-wire anemometer. Thus summary of those results are documented in the following.

Free-stream turbulence intensity Tu_b decreases along with the distance measured from the turbulence grid. It was found that this could be described by the following expression for each type of the turbulence grids used in this study.

$$Tu_b = 10.64\left((L-|x|)/M\right)^{-0.559}, \quad M/d_g \cong 6 \tag{6}$$

where L is the distance between the turbulence grid and the test model. Eq. (7) was modified in order to account for the blockage effect of the test model upon the turbulence intensity, which resulted in the following expression;

$$Tu_b(x) = 10.64\left((L-|x|)/M\right)^{-0.559} \times \frac{1}{1-\left(R/(x-R)\right)^2}. \tag{7}$$

Conventionally a reference free-stream turbulence intensity is defined as the minimum value calculated from Eq. (7).

Wake turbulence was measured likewise in the free-stream turbulence case and the data was arranged in terms of peak turbulence intensity within the wake as follows;

$$Tu_{\max} = 73.58\left((l-|x|)/d\right)^{-0.67}, \tag{8}$$

where l is the distance between the wake-generating moving plane and test model. It is recently found that Eq. (8) yields almost the same results as the experimental data given by Halstead et al[9].

As for length scale of the free-stream turbulence, a streamwise turbulence dissipation scale L_e, defined as (Hancock and Bradshaw[10])

$$L_e = -\frac{(\overline{u'^2})^{3/2}}{U\, d\overline{u'^2}/dx} \tag{9}$$

can be calculated by use of Eq. (6).

In the nominal setting of the test model L is 300 mm and l is 200 mm and a reference free-stream turbulence and its dissipation length are accordingly determined as documented in Table 1.

Views of Temperature Distributions by Liquid Crystal

Figure 6 shows three images of temperature distributions near the cooling holes captured by the liquid crystal under no artificial flow disturbances for $B = 0.4$, 0.8 and 1.2, respectively. For the lowest blowing ratio, as indicated in Figure 4, very small amount of the secondary air is injected from the cooling hole in the first row. Moreover, the injected air from the second row is convected almost horizontally along the model surface, covering a limited

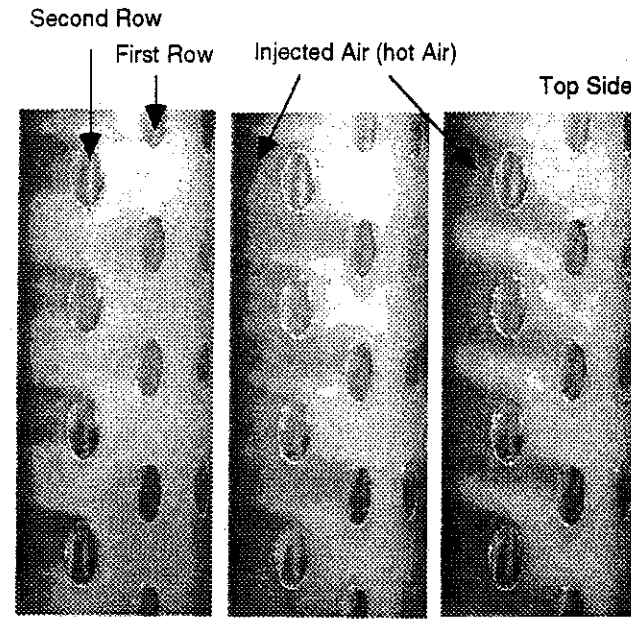

Figure 6 Views of temperature distributions near the cooling holes obtained by the liquid crystal (No Grid / S = 0)

area on the entire model surface. For $B = 0.8$, injected air from the upper half of the cooling hole in the first row can be identified, which moves and spreads so as to cover the area between the neighboring cooling holes in the second row. Eventually the injected air together with that from the second row covers almost the entire surface after the second row, implying that this blowing ratio will yield high values of spanwise averaged film effectiveness. For the highest blowing ratio $B = 1.2$, because of its high spanwise momentum flux, the injected air is gradually drifted in the spanwise direction along the model surface. One might notice that mergers happen between the injected airs from the first and the second rows, which ends up with the appearance of uncovered regions by the injected air.

Local Film Effectiveness Distribution

General features. Figure 7 shows local film effectiveness distributions on the unfolded surface of the test model for three blowing ratios in the "no wake ($S = 0$)" condition with low free-stream turbulence (No Grid), accompanied by rough sketches indicating the coverage of the injected airs from the cooling holes. Note that the bottom line of the unfolded surface in Figure 7 corresponds to the top line of Figure 3. Therefore, y coordinate in Figure 7 is directed toward the bottom of the test model.

Figure 7 reveals clear relationship between the injected air and high or low film effectiveness appearing on each measuring location. For $B = 0.4$, since only a small amount of secondary air comes from the cooling holes in the first row, the film effectiveness at the downstream of a hole in the first row is low. On the other hand, the film effectiveness at the downstream of a hole in the second row, especially at the upper side of the cooling hole, becomes considerably high, which results in large spanwise variation of the film effectiveness. For $B = 0.8$, the injected air covers almost the entire surface of the test model, so that we obtain relatively high values of film effectiveness over the surface. For $B = 1.2$, the injected air drifts towards the top side of the test model and eventually there appear regions behind the second row that are not covered by the injected air. This results in significant spanwise variation in film effectiveness at the downstream of the second row. Observations from an another view angle also shows that the injected air tends to

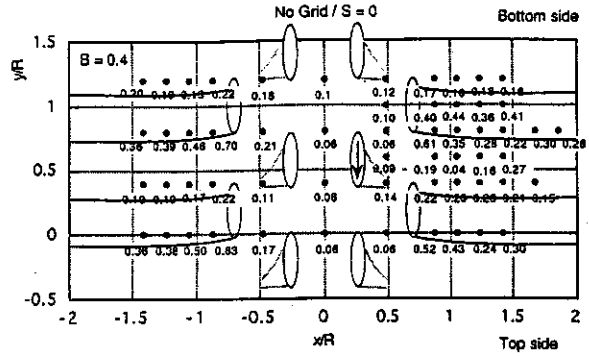

B = 0.4

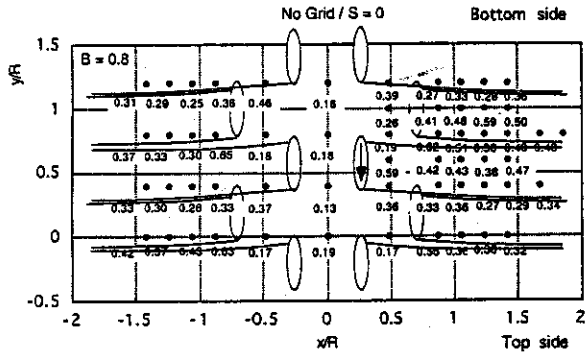

B = 0.8

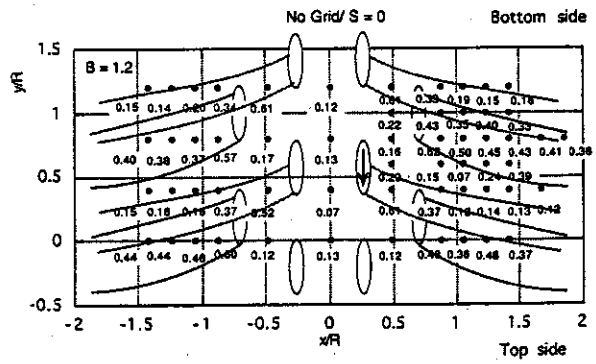

B = 1.2

Figure 7 Local film effectiveness distributions near the holes with sketches of the coverage of the injected air (No Grid / S = 0)

spread on the surface and those uncovered regions gradually disappear towards the aft portion of the test model.

Effect of the wake passing. Figure 8 shows the local film effectiveness distribution for $B = 0.8$ under the influence of the wake passage ($S = 0.40$). Note that the lines drawn in this figure is the same as those in Figure 7 only for convenience. A comparison between Figure 8 and Figure 7 shows that the wake passage significantly deteriorates the film effectiveness. Close inspections reveal that the film effectiveness measured along the horizontal line passing the center of the hole reduces by 10 - 20%, while the

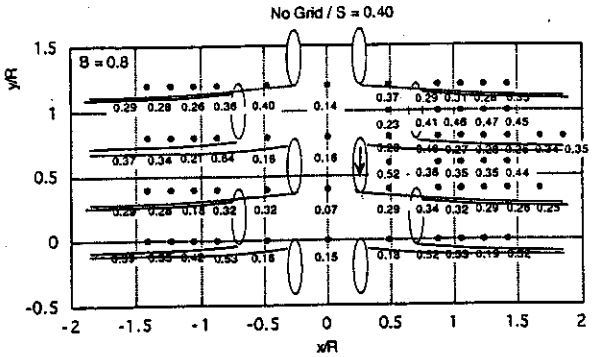

Figure 8 Effect of wake passing on the local film effectiveness distributions near the holes (B=0.8 / No Grid / S = 0.40)

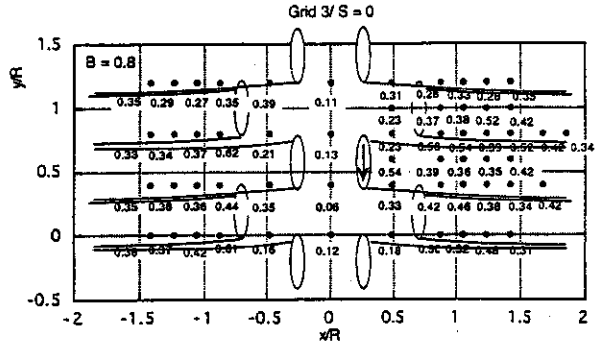

Figure 9 Effect of free-stream turbulence on the local film effectiveness distributions near the holes (B= 0.8 / Grid 3 / S = 0)

film effectiveness measured near the fringe of the injected air reduces by 10% at most. One of the plausible explanations on this phenomena might be the wake-enhanced mixing of the mainstream with the injected air, however, we cannot deny a possible contribution of wake-induced variation in local mass flux from each of the cooling holes to the film effectiveness. Detailed measurement on this flow field is strongly required.

Effect of free-stream turbulence. Figure 9 shows the local film effectiveness distribution for $B = 0.8$ under the influence of the free-stream turbulence (Grid 3). A comparison between Figure 9 and Figure 7 shows that the augmented free-stream turbulence tends to reduce the film effectiveness over the surface, however, there even appears a slight increase in film effectiveness near the fringes of the injected air, in contrast to the wake passing case mentioned above. Similar phenomena were already observed by Mehendale and Han[1], where a ratio of hole pitch to hole diameter was 3. Although it is difficult to generalize this result due to the uncertainty contained, spanwise mixing seemingly enhanced by the free-stream turbulence contributes to the local increase in film effectiveness.

Spanwise Averaged Film Effectiveness

General features. Figure 10 shows the plots of spanwise averaged film effectiveness for three blowing ratios under the influence of the wake passing. It should be noted that the obtained film effectiveness distributions are not symmetric with respect to

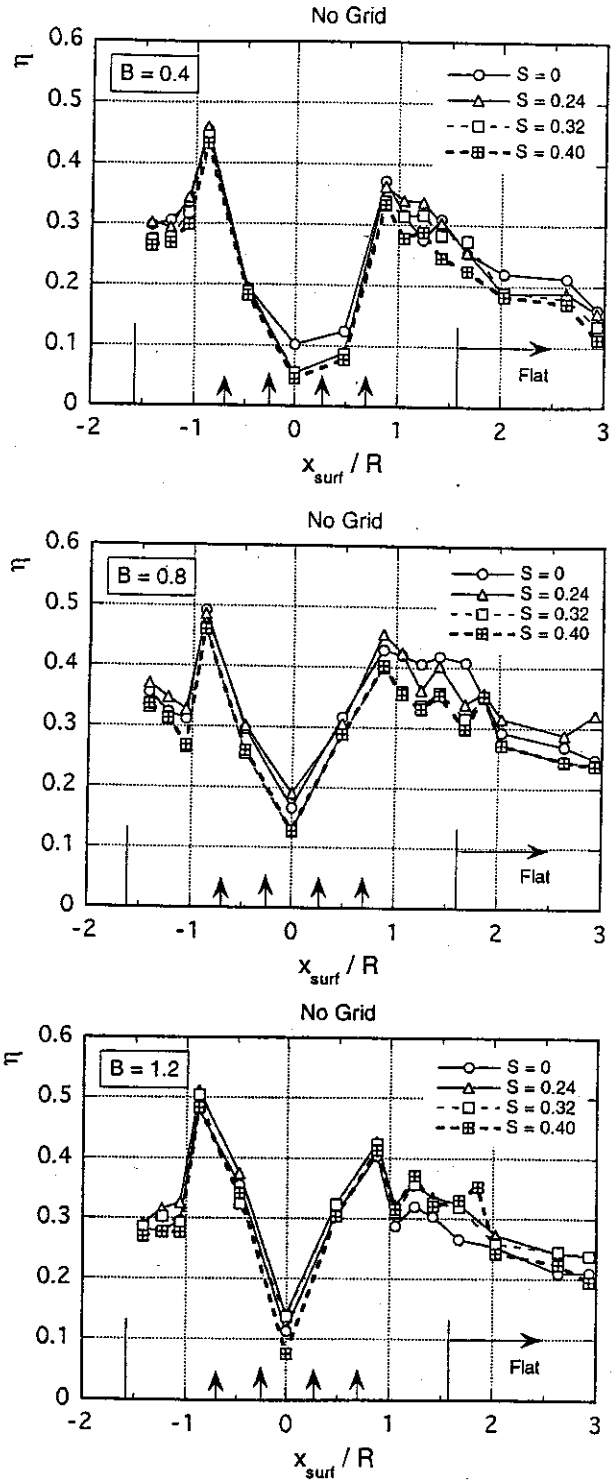

Figure 10 Effect of wake passage upon the spanwise averaged film effectiveness for three blowing ratios (No Grid)

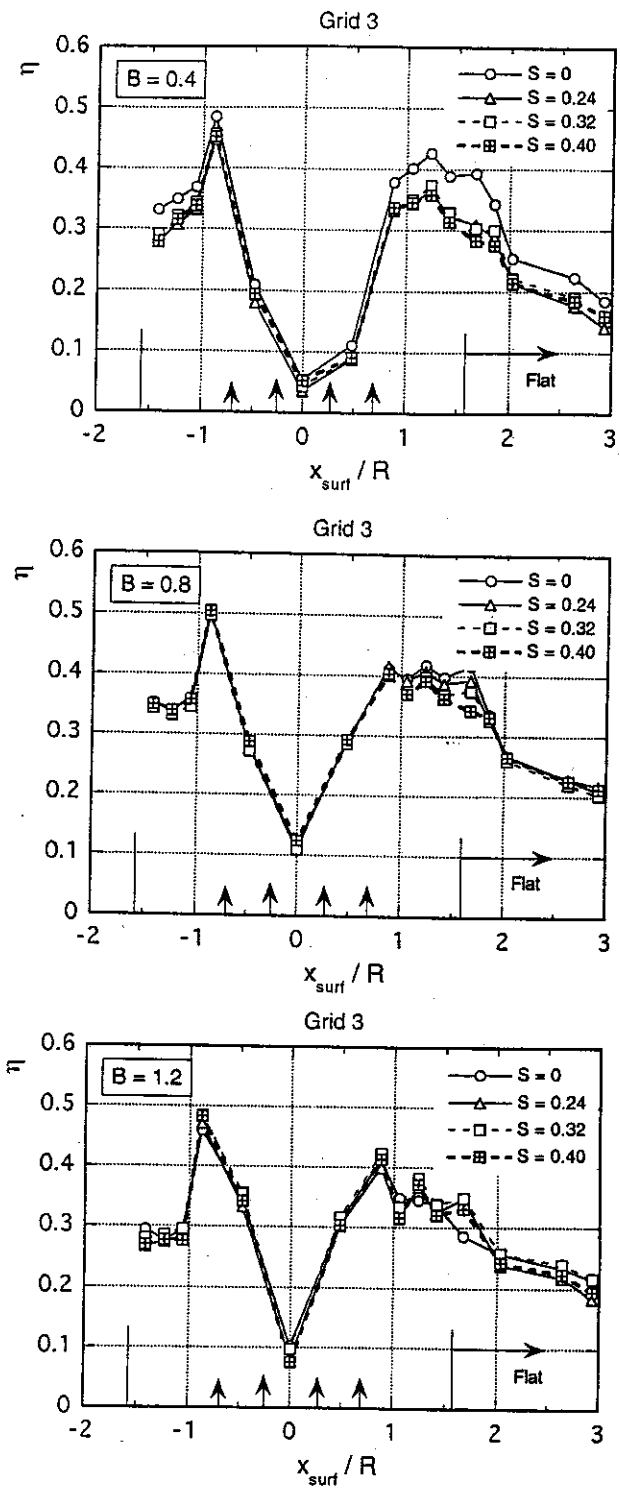

Figure 11 Effect of wake passage upon the spanwise averaged film effectiveness for three blowing ratios (Grid 3)

the stagnation line, $x_{surf}/R = 0$, especially for $B = 0.4$. This is mainly because of the difference in sample number for averaging, as shown in Figure 3. Moreover, it seems that mass flow rates from the holes at +15° and −15° are not the same each other in this lowest blowing ratio, which contributes to this asymmetry. Hereafter the discussion is focused on the data on the right-hind side($x_{surf}/R \geq 0$) of these plots.

Generally the maximum appears after the second row of the film holes, followed by gradual decrease due to the dilution. For $B = 0.8$, this decreasing rate is relatively slow compared to other cases, which results in the highest spanwise average film effectiveness over the model surface among three blowing ratio cases, as can be expected from the local film effectiveness distributions. In the case of $B = 1.2$, there appears a small valley of the film effectiveness after the maximum, probably due to the spanwise variation of the local film effectiveness as identified in the above.

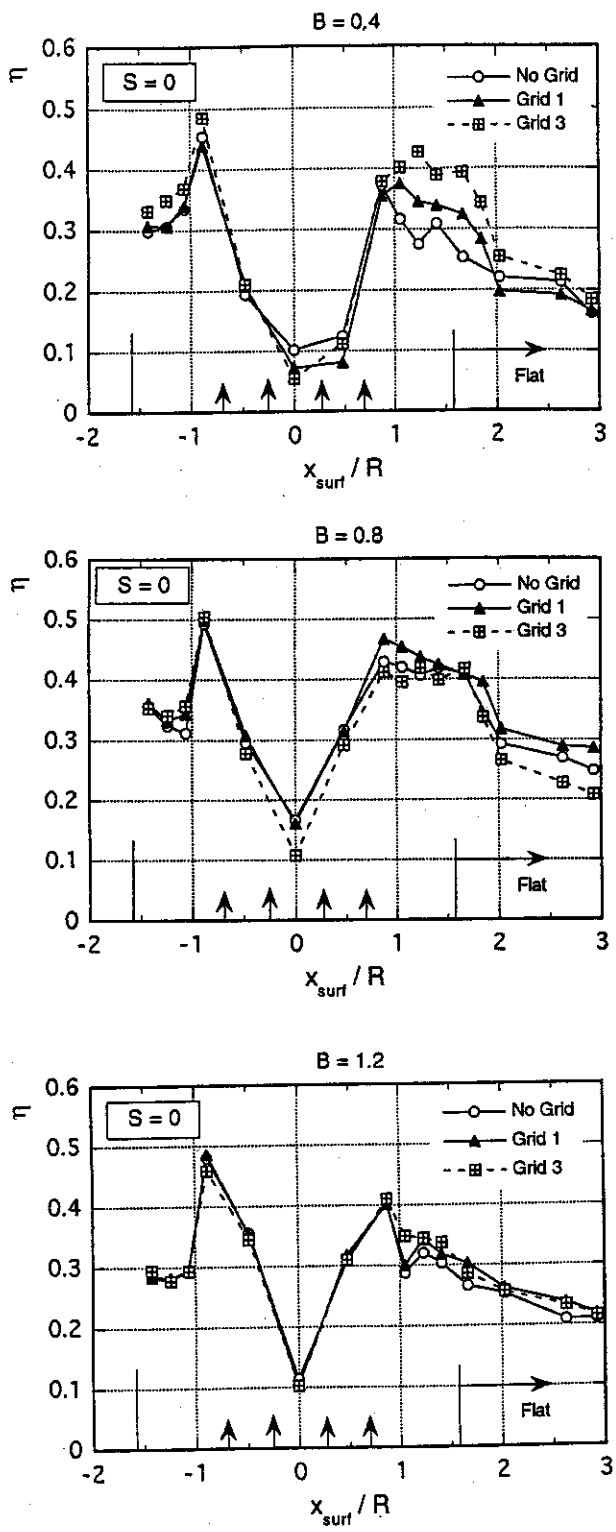

Figure 12 Effect of enhanced free-stream turbulence on the spanwise averaged film effectiveness for three blowing ratios (S = 0)

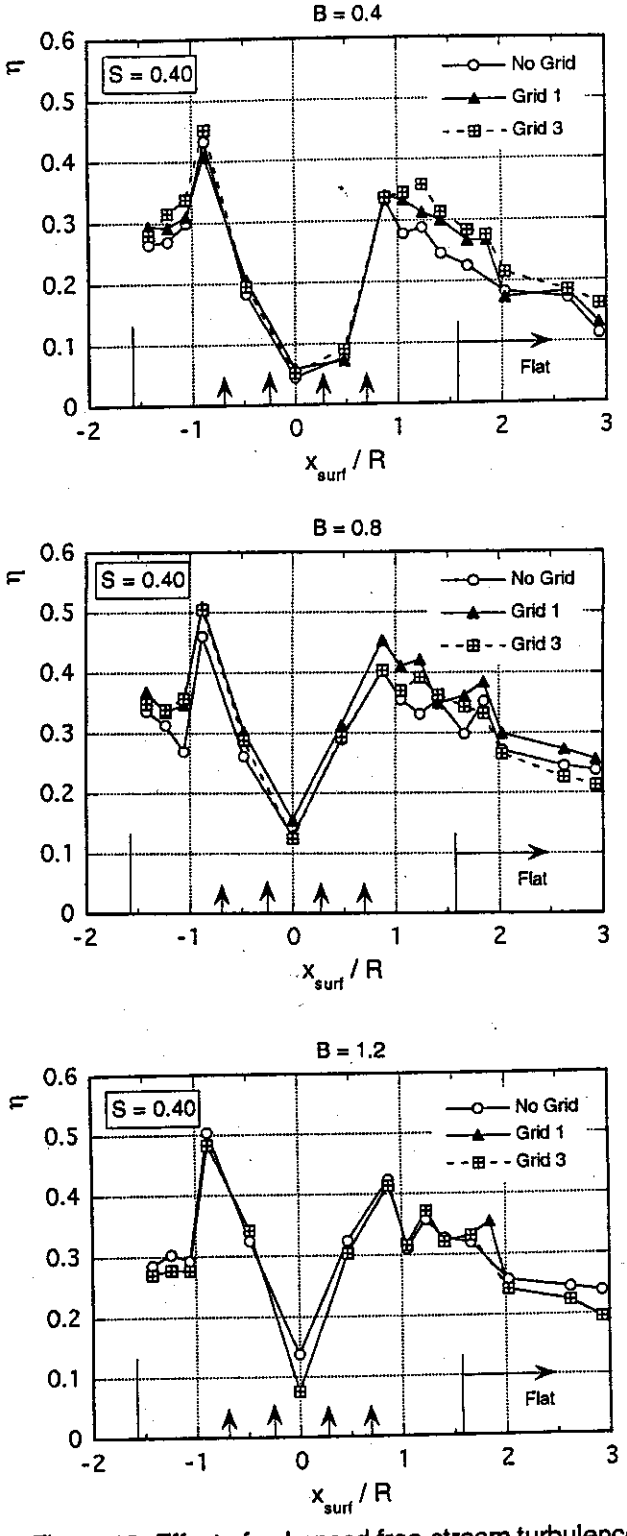

Figure 13 Effect of enhanced free-stream turbulence on the spanwise averaged film effectiveness for three blowing ratios (S = 0.40)

Effect of the wake passage. As the Strouhal number increases, the averaged film effectiveness tends to decrease for $B = 0.4$ and $B = 0.8$. However, for $B = 1.2$, the averaged film effectiveness rather exhibits a slight increase, as seen in the local film effectiveness distribution.

Figure 11 shows spanwise averaged film effectiveness under the influence of the wake passing as well as enhanced free-stream turbulence from Grid 3. Except for the case of $B = 0.4$ and the data obtained around the separation zone for $B = 0.8$, no discernible effect of the wake passage upon the average film effectiveness can be found. As for the case of $B = 0.4$, the reason of the notable decrease in the averaged film effectiveness with the increase of Strouhal number it is not certain. However, it can be concluded that the wake passage over the test model reduces the film effectiveness in the case of low and moderate blowing ratios.

Effect of free-stream turbulence. Figures 12 and 13 show the effect of free-stream turbulence on the spanwise average film effectiveness for three blowing ratios without and with the influence of the periodic wakes. It follows from these data that, regardless of the influence of the wake passage, free-stream turbulence does not have any significant impact on the spanwise average film effectiveness for $B=1.2$. For the case of $B=0.4$, augmented free-stream turbulence surprisingly increases the averaged film effectiveness over the region ranging from x_{surf}/R=1 - 2. Note that this region almost corresponds to the area where the separation occurs. Despite the influence of the wake passing, this tendency does not change, where the effect of the free-stream turbulence becomes small though (see Figure 13). For a moderate blowing ratio $B=0.8$, the enhanced free-stream turbulence appears to decrease the average film effectiveness to some extent, however, its effect almost diminishes under the influence of the wake passage.

CONCLUSIONS

Detailed studies were conducted on film effectiveness of inclined discrete film holes around the leading edge of a blunt test model of a turbine blade that was subjected to periodically incoming wakes as well as free-stream turbulence with various levels of intensity. Important findings, useful for designing film-cooled turbine blades, were obtained in the studies. Summary of this paper is itemized as follows;

1. Observations by use of the liquid crystal revealed the extent of film coverage near the film holes at the leading edge. At the lowest blowing ratio $B=0.4$, the secondary air from the film holes in the first row could not be identified and the air from the holes in the second row was convected almost horizontally. At the blowing ratio $B=0.8$, the injected air from the holes in the first and the second rows tended to cover almost the entire surface of the test model behind the second row. Further increase in blowing ratio caused spanwise drift of the injected air, which led to an appearance of uncovered region by the injected air.
2. From the local film effectiveness distributions, accompanied by the sketches of the injected air trajectories, it was found the blowing ratio $B=0.8$ produced relatively small spanwise variation in film effectiveness compared to the other blowing ratio cases. This was because the injected secondary air achieved almost full coverage situation.
3. Under the influence of periodic wake passage, the local film effectiveness tended to deteriorate by 10 - 20% at the centerline of the hole exit area. In contrast, the augmented free-stream turbulence did not always decrease the spanwise averaged film effectiveness, in some cases the film effectiveness increased probably due to the enhanced spanwise mixing effect.
4. Generally, distributions of the spanwise averaged film effectiveness exhibited the maximum just behind the second row, followed by gradual decrease towards the downstream. On the average, the blowing ratio $B=0.8$ yielded relatively high film effectiveness. Periodic wake passage usually deteriorated the spanwise film effectiveness. On the other hand, enhanced free-stream turbulence did not always deteriorated the film effectiveness drastically, sometimes it rather caused a slight increase in the film effectiveness. The effect of the free-stream turbulence tended to diminish with the increase in Strouhal number.

ACKNOWLEDGMENTS

The authors are greatly indebted to Mr. M. Yokota, former graduate student of Iwate University, for his contribution to the present study.

REFERENCES

[1] Mehendale, A.B., and Han, J.C., "Influence of High Mainstream Turbulence on Leading Edge Film Cooling Heat Transfer," ASME *Journal of Turbomachiney*, Vol. 114, 1992, 707-715

[2] Takeishi, K., Aoki, S., Sato, T, and Tsukagoshi, K., "Film Cooling on a Gas Turbine Rotor Blade," ASME *Journal of Turbomachinery*, Vol. 114, 1992, 828-834.

[3] Mehendale, A.B., Han, J.C., Ou, S., and Lee., C.P., "Unsteady Wake Over a Linear Turbine Blade Cascade with Air and CO_2 Film Injection: Part II - Effect on Film Effectiveness and Heat Transfer Distributions," ASME Paper No. 93-GT-134, 1993

[4] Funazaki, K., Yamawaki, S. and Maya, T., "Studies on Wake-Affected Heat Transfer around the Leading Edgeof a Blunt Body (Effect of Free-Stream Turbulence)," Proceedings of ASME/JSME Thermal Engineering Conference, Vol. 1, 343-350

[5] Funazaki, K., Yokota, M. and Yamawaki, S., "The effect of Periodic Wake Passing on Film Effectiveness of Discrete Cooling Holes around the Leading Edge of a Blunt Body," ASME Paper No. 95-GT-183

[6] Funazaki, K., "Studies on Wake-Affected Heat Transfer Around the Circular Leading Edge Blunt Body," ASME Paper No. 94-GT-25, 1994.

[7] Mick,W.J. and Mayle,M.E., "Stagnation Film Cooling and Heat Transfer, Including Its Effect within the Hole Pattern," ASME *Journal of Turbomachinery*, Vol. 110,1988, 66-72

[8] Kline, S.J. and McClintock, F.A., "Describing Uncertainties in Single Sample Experiments," *Mechanical Engineering*, Vol. 75, 1953, 3-8.

[9] Halstead, D.E., Wisler, D.C., Okiishi, T.H., Walker, G.J., Hodson, H.P. and Shin, H.W., "Boundary Layer Development in Axial Compressor and Turbines, Part 4 of 4: Computations and Analysis," ASME Paper 95-GT-464, 1995

[10] Hancock, P.E. and Bradshow, P., "The Effect of Free-Stream Turbulence on Turbulent Boundary Layers," ASME *Journal of Fluids Engineering*, Vol. 105, 1983, 284-289